Ammonia Dehydrogenation over Platinum-Group Metal Surfaces. Structure, Stability, and Reactivity of Adsorbed NH x Species

ARTICLE *in* THE JOURNAL OF PHYSICAL CHEMISTRY C · JANUARY 2007

Impact Factor: 4.77 · DOI: 10.1021/jp064742b

Ammonia Dehydrogenation over Platinum-Group Metal Surfaces. Structure, Stability, and Reactivity of Adsorbed NH_x Species

Gerard Novell-Leruth,[†] Ana Valcárcel,[†] Javier Pérez-Ramírez,[‡,§] and Josep M. Ricart*,[†]

Departament de. Química Física i Inorgànica, Universitat Rovira i Virgili, C/Marcel.lí Domingo s/n, 43007 Tarragona, Spain, Institute of Chemical Research of Catalonia (ICIQ), Av. Països Catalans 16, 43007 Tarragona, Spain, and Catalan Institution for Research and Advanced Studies (ICREA), Pg. Lluís Companys 23, 08010 Barcelona, Spain

Received: July 25, 2006; In Final Form: October 4, 2006

Periodic DFT calculations using plane waves have been applied to comparatively study the adsorption and decomposition of ammonia on the (111) and (100) surfaces of platinum-group metals (Pd, Rh, Pt). Different adsorption geometries and positions have been studied for NH_3 and its dehydrogenation intermediates (NH_x, $x = 0, 1, 2$). On the six surfaces investigated, NH_3 adsorbs preferentially on top sites, NH_2 on bridge, and NH and N on hollow sites. However, the adsorption energies of the NH_x moieties differ considerably from one surface to another. All of the species adsorb more strongly on the (100) than on the (111) planes. Rh(100) provides the maximum stability for the various intermediates. The reaction energies, the structure of the transition states, and the activation barriers of the successive dehydrogenation steps ($NH_x \rightarrow NH_{x-1} + H$) have been determined, making it possible to compute rate coefficients at different temperatures. Our calculations have confirmed that ammonia decomposition over noble metal catalysts is structure sensitive. As a general trend, the first dehydrogenation step is rate determining, especially for Pd. In agreement with experiments, Rh is a better catalyst for NH_3 decomposition than are Pt and Pd. The former strongly stabilizes the highly dehydrogenated NH and N species and also leads to the lowest activation barriers. For the set of dehydrogenation reactions, a linear relationship between the transition state potential energy and the adsorption energy of the final state has been obtained.

1. Introduction

Catalytic conversions involving ammonia are of great relevance in the chemical industry. Accordingly, the interaction of ammonia with metal surfaces (particularly Fe, Ni, Cu, Ag, Pt, Ir, or Ru) has been thoroughly investigated.[1] Many of these studies were primarily undertaken to gain insight into the synthesis of ammonia. However, other processes, such as the oxidation of ammonia in nitric acid production,[2] the reaction of ammonia with methane to produce HCN,[3] and more recently the decomposition of ammonia to produce high-purity H_2 for fuel cells,[4−6] are of high practical importance too.

In particular, platinum-group metals (PGM) and their alloys are superior catalysts for ammonia oxidation to NO (Ostwald process) and in the synthesis of HCN via the $NH_3 + CH_4$ reaction in the absence (Degussa process) or presence (Andrussow process) of O_2. Experimental assessment of the surface chemistry related to these reactions is intricate due to the demanding conditions of temperature and pressure and the very fast kinetics, which make the identification of elementary steps and key reaction intermediates unfeasible.

Application of surface science techniques in UHV over platinum single crystals in a broad temperature range (300−1700 K),[7−14] and more recently the Temporal Analysis of Products (TAP) reactor over commercial Pt and Pt−Rh gauzes at 973−1173 K,[15−17] have provided valuable insights into the mechanism of the high-temperature ammonia oxidation. These studies demonstrated that the oxidation is initiated by dehydrogenation of the ammonia molecule by adsorbed oxygen atoms, leading to reactive NH_x intermediates. According to the hydride mechanism, the latter fragments end up in reaction products by further H-stripping, O-transfer into NH_x intermediates (forming NO), and coupling of N-species (forming N_2 and N_2O). However, despite many dedicated studies, a generally accepted atomic-level description as well as a systematic characterization of intermediate NH_x species has not been achieved as yet. This information sets the basis for deriving rational microkinetic models able to predict the performance of PGM catalysts in ammonia conversion.

On Pt(111) and Pt(100) surfaces, TPDS, HREELS, AES, and LEED studies in ultrahigh vacuum have shown that NH and NH_2 species are intermediates in ammonia oxidation.[8,10] HREELS and TPRS studies also identified NH_2 species in the reaction between H and NO on Pt(100)-(1 × 1).[18] The various NH_x fragments have been also evidenced on Pt(111) upon electron bombardment of molecularly adsorbed ammonia at 100 K.[19,20] These authors have reported that adsorbed NH_2 species are dominant at subambient temperature. Dissociation of these species occurs in the temperature range of 300−400 K, and NH becomes the main surface species. On further heating, adsorbed NH dissociates and N_2 desorbs. Yamada and Tanaka, using HREELS, have also detected NH_x species while exposing a c(2 × 2)-N overlayer on Pd(100),[21,22] $Pt_{0.25}Rh_{0.75}$(100),[23] and Rh(100)[24] to H_2. They have concluded that the main surface species is NH, which is in line with the results by Herzeg et al.[25] The latter authors have investigated the formation and

* Corresponding author. E-mail: josep.ricart@urv.cat.
[†] Universitat Rovira i Virgili.
[‡] Institute of Chemical Research of Catalonia (ICIQ).
[§] Catalan Institution for Research and Advanced Studies (ICREA).

10.1021/jp064742b CCC: $37.00
Published on Web 11/18/2006

dissociation chemistry of NH species on Pt(111) by using RAIRS and TPDS techniques.

Theoretical ab initio approaches based on quantum chemical principles can contribute to a rational description of the complex ammonia dehydrogenation process. Despite outstanding theoretical studies in the topic of ammonia synthesis over a number of surfaces,[26−28] only few theoretical works have systematically examined the fragmentation of adsorbed NH_x species on Pt(111),[29−31] Pd(111),[32] and Rh(111).[33] In fact, ammonia dehydrogenation studies over (100) surfaces are to the best of our knowledge not reported in the literature.

Our recent work[30] assessed the adsorption and relative stability of ammonia and the resulting dehydrogenated NH_x species ($x = 0, 1, 2$) on Pt(111) and Pt(100) surfaces using periodic slab DFT calculations. NH_3 and NH_2 were found to be more stable on Pt(100) than on Pt(111), while NH and N exhibited similar stabilities. A remarkable difference was found for NH_2, being ca. 68 kJ mol^{-1} more stable on Pt(100). On the basis of this, it was suggested that the dehydrogenation of ammonia on platinum is structure sensitive. This theoretical prediction has been substantiated in recent experimental work by Vidal-Iglesias et al.,[34] showing that the electrocatalytic oxidation of ammonia takes place almost exclusively on Pt(100) sites. In line with this, Rosca and Koper[35] have reported very different electrocatalytic NH_3 oxidation activities between Pt(100) and Pt(111), and related the higher rate of N_2 production over Pt(100) with the stabilization of the NH_2 adsorbate. On Pt(100), NH and N adsorbed species are stabilized, and reaction practically does not occur. More recently, Offermans et al.[31] have provided by means of DFT new mechanistic and kinetic insights into the ammonia oxidation on Pt(111), including also the NH_x dehydrogenation reactions.

Following our previous study,[30] this work systematically investigates the non-oxidative dehydrogenation of ammonia over PGM surfaces. The structure, stability, and reactivity of adsorbed NH_3, NH_2, NH, N, and H species have been comparatively analyzed over the (100) and (111) surfaces of the Pt, Rh, and Pd. The analogies and differences presented here comprise a first requisite to subsequently approach the influence of oxygen in the reaction.

2. Computational Details

Calculations were performed in the frame of DFT using the Vienna Ab Initio Simulation Program (VASP).[36,37] This program solves the Kohn−Sham equations of the density functional theory with the development of the one-electron wave function in a basis of plane waves. The electron−ion interactions were described by the projector augmented wave (PAW) method.[38] The tight convergence of the plane-wave expansion was obtained with a cutoff of 400 eV. The generalized gradient approximation (GGA) was used with the functional of Perdew and Wang.[39] We considered the 2×2 unit cell associated with a molecular coverage of 1/4 ML. The 2D Brillouin integrations were performed on a $5 \times 5 \times 1$ grid. The correct convergence of the adsorption energy by using this density of k-points was evaluated. For adsorbed NH_x fragments ($x = 0-2$), a non-polarized spin formalism was used because spin polarization effects were found to be negligible.

The (100) and the (111) metal surfaces were modeled by a two-dimensional slab in a three-dimensional periodic cell generated by introducing a vacuum width of ca. 12 Å in the normal direction to the surface. The slabs contained four atomic metal layers with the target molecule and atomic species (NH_3, NH_2, NH, N, and/or H) adsorbed on one side of the slab. The optimized metal−metal interatomic distances for the bulk were used to prevent false forces on the metal atoms. The resulting calculated values (2.82 Å Pt−Pt, 2.80 Å Pd−Pd, and 2.72 Å Rh−Rh) were indeed close to those determined experimentally (2.77, 2.75, and 2.69 Å, respectively).[40] The energy of the bare surfaces was calculated permitting relaxation of the two top layers.

The geometry optimization included all degrees of freedom of the adsorbates and the two uppermost metal layers, while the two lowest metal planes were fixed at the optimized bulk geometry. The adsorption energy (E_{ads}) was computed as the difference between the energy of the adsorbed molecule ($E_{NH_x-surface}$) and the sum of the free surface ($E_{surface}$) and the corresponding gas-phase species ($E_{gas-phaseNH_x}$) energies according to eq 1.

$$E_{ads} = E_{NH_x-surface} - E_{surface} - E_{gas-phaseNH_x} \quad (1)$$

A negative value of E_{ads} indicates an exothermic chemisorption process. To compare the relative stabilities of the different species, the adsorption energies were recalculated with respect to a common reference system: the NH_3 molecule in the gas phase (eq 2). We considered that the adsorbed NH_x species and $(3 - x)$H atoms do not interact; that is, they are separated by infinite distance.

$$E_{rel} = (E_{NH_x-surface} + (3 - x)E_{H-surface}) - ((4 - x)E_{surface} + E_{gas-phaseNH_3}) \quad (2)$$

Reaction energies for the successive $NH_x \rightarrow NH_{x-1} + H$ ($x = 1-3$) dehydrogenation steps were computed in two ways depending on the selection of the final state and are denoted as ΔE_1 and ΔE_2. In ΔE_1, the reaction products were coadsorbed on the same cell, whereas in ΔE_2 the NH_{x-1} fragment and the H atom were at infinite distance on the surface.

The Dimer method[41] was used to determine the transition states. The obtained results were refined until a negligible value of the forces with the quasi-Newton algorithm implemented in VASP.

A full vibrational analysis was conducted to check the validity of both the optimized geometries and the determined transition states. The dynamical matrix was obtained by numerical differentiation of the forces and diagonalized, providing the harmonic molecular frequencies and the normal modes. These calculations made it possible (1) to include the zero point energy, ZPE (eq 3),

$$ZPE = \sum_i ({}^1/_2)h\nu_i \quad (3)$$

where ν_i are the computed real frequencies of the system, and (2) to calculate the rate coefficients (k_v) for the different elementary steps during ammonia dehydrogenation using the transition state theory in the harmonic approach:

$$k_v = \frac{kT}{h}\frac{Z_{TS}}{Z_{IS}}e^{-E_a/kT} = k^0 e^{-E_a/kT} \quad (4)$$

where Z_{IS} and Z_{TS} are the partition functions in the initial and transition states, respectively. In this equation, E_a is the ZPE-corrected activation energy, k^0 is the pre-exponential factor, and k and h are the Boltzmann and Planck constants, respectively. Because NH_3 adsorbed on top sites behaves as a nearly free

TABLE 1: Adsorption Energies (in kJ mol^{-1}) of the Different Fragments with Respect to Each Species in the Gas Phase; Distance from N to the Closest Metal Atom (d_{M-N}), N−H Distance (d_{N-H}), and Height from the Surface Layer (z) (Distances in angstroms)

	Pt(100)	Pd(100)	Rh(100)	Pt(111)	Pd(111)	Rh(111)
			NH_3			
site	top	top	top	top	top	top
E_{ads}	−76	−64	−82	−68	−55	−76
E_{ads} (ZPE)[a]	−66	−56	−73	−58	−46	−66
d_{M-N}	2.13	2.17	2.15	2.16	2.18	2.15
d_{N-H}	1.02	1.02	1.02	1.02	1.02	1.02
z	2.13	2.17	2.15	2.15	2.17	2.15
			NH_2			
site	bridge	bridge	bridge	bridge	bridge	bridge
E_{ads}	−300	−266	−321	−241	−235	−278
E_{ads} (ZPE)	−279	−248	−302	−221	−217	−260
d_{M-N}	2.06	2.06	2.06	2.09	2.07	2.08
d_{N-H}	1.02	1.02	1.02	1.02	1.02	1.02
z	1.42	1.45	1.52	1.52	1.51	1.59
			NH			
site	hollow	hollow	hollow	fcc	fcc	hcp
E_{ads}	−378	−407	−489	−406	−387	−443
E_{ads} (ZPE)	−360	−390	−472	−385	−363	−426
d_{M-N}	2.18	2.12	2.13	2.01	1.99	2.01
d_{N-H}	1.03	1.03	1.03	1.02	1.03	1.02
z	0.91	0.81	0.93	1.07	1.08	1.19
			N			
site	hollow	hollow	hollow	fcc	fcc	hcp
E_{ads}	−422	−486	−561	−467	−451	−516
E_{ads} (ZPE)	−417	−478	−554	−458	−441	−508
d_{M-N}	2.11	2.02	2.04	1.96	1.92	1.92
z	0.75	0.05	0.68	1.01	1.00	1.05
			H			
site	bridge	hollow	hollow	fcc	fcc	fcc
E_{ads}	−276	−263	−275	−266	−281	−276
E_{ads} (ZPE)	−260	−257	−267	−252	−264	−260
d_{M-H}	1.76	1.99	2.01	1.87	1.81	1.86
z	1.02	0.34	0.60	0.86	0.79	0.96

[a] ZPE included.

2D rotator, its lowest frequency mode was considered as a rotation in the calculation of the partition functions.[31]

3. Results and Discussion

3.1. Adsorption of Ammonia. Ammonia was systematically adsorbed on different sites for each surface, that is, top, bridge, and hollow for (100) and top, bridge, and hollow fcc or hcp for the (111) surfaces. Adsorbed NH_3 was found to be favored on top sites on all metal surfaces, bound via the N atom and with the H atoms pointing outward. Any attempt to find a minimum of energy in the other symmetric sites led to the on top site after complete optimization, in agreement with previous theoretical studies of ammonia adsorption on transition metals.[42−46] The adsorption energies are presented in Table 1. Results corresponding to the Pt surfaces were presented and discussed in a previous paper,[30] but are included here to establish a comprehensive comparison with the other platinum-group metals.

The values obtained for NH_3 adsorbed on Rh(100) (−82 kJ mol^{-1}, −73 kJ mol^{-1} ZPE corrected) and Rh(111) (−76 kJ mol^{-1}, −66 kJ mol^{-1} ZPE corrected) are in line with the earlier results reported by Liu et al.[33] and by Frechard et al.[47] using similar methods and models, and the results for Pd are in good agreement with the experimentally determined heat of adsorption on Pd foils (−72 kJ mol^{-1}).[48] The zero point energy correction reduces the value of the adsorption energy by ∼10 kJ mol^{-1}. The adsorption energy on the (100) surface is always higher than that on the (111) surface for all of the metals, although the differences between the two planes over the same metal are relatively small (<12 kJ mol^{-1}). The order of stability of adsorbed ammonia on the metals is Rh > Pt > Pd. Among all of the minima (Table 1), there are no significant differences in the metal−nitrogen distances (d_{M-N}), which are about 2.15 Å, and the N−H distances (1.020 Å) do not change with respect to those in the gas phase (1.024 Å).

3.2. Adsorption of NH_x Fragments. Table 1 shows the adsorption energies and geometrical parameters of the various NH_x fragments ($x = 0-2$) on their more stable adsorption site. The other sites lead to less stable adsorbed states or are not minima. All of the species chemisorb molecularly in a N-down orientation. NH_2 preferentially adsorbs on the bridge site, with the molecular C_2-axis perpendicular to the surface, whereas NH and N prefer the hollow sites on both (100) and (111) surfaces. The main difference is that the most stable adsorption site is the hollow hcp on Rh(111), whereas the hollow fcc is the preferred one on Pt(111) and Pd(111). However, the energy difference between the two hollow sites is rather small. On Rh the hcp site is the preferred one only by 2 kJ mol^{-1} (NH) and 12 kJ mol^{-1} (N). On Pt and Pd, the fcc is the preferred adsorption site by 38 and 18 kJ mol^{-1} for NH and by 27 and 13 kJ mol^{-1} for N, respectively. A small hcp−fcc energy gap suggests that both sites are populated to a similar extent. Besides, this fact shows that the second metal layer does not significantly influence the adsorption. We anticipate that the transition states will follow the same trends, and we took the most stable sites for further calculations. Our results for both preferred adsorption

TABLE 2: Adsorption Energy (kJ mol^{-1}) of Atomic Hydrogen on the Symmetric Sites of the Surfaces[a]

	top	bridge	hollow
Pt(100)	−35	−54	−31[b]
Pd(100)	1[b]	−40	−50
Rh(100)	−25[b]	−53	−60

	top	bridge	hcp	fcc
Pt(111)	−39	−42	−42	−46
Pd(111)	−9[b]	−46[c]	−54	−58
Rh(111)	−18	−44[c]	−51	−54

[a] Energies were computed with respect to the gas-phase H_2 molecule and include the ZPE correction. [b] Second-order saddle point. [c] First-order saddle point.

site and binding energy are in good agreement with data available in the literature: N on Rh(111), −521 kJ mol^{-1} [49] and −493 kJ mol^{-1};[50] N on Pt(100), −414 kJ mol^{-1};[51] N on Rh-(100), −548 kJ mol^{-1};[51] NH_2, NH, N on Pt(111), −298, −387, and −449 kJ mol^{-1} [31] or −221, −369, and −420, respectively;[52] NH_2, NH, N on Rh(111), −263, −423, and −473 kJ mol^{-1}.[33]

As observed for NH_3, the adsorption energies of the fragments (Table 1) are generally higher on the (100) surface than on the (111) surface for the different metal surfaces. As a general trend, the order of stability is Pd(111) < Pt(111) < Pd(100) < Rh-(111) < Pt(100) < Rh(100), although NH and N on Pt(100) are less stable than expected following this tendency, as discussed elsewhere.[30] The surface providing maximum stability to the adsorbed species is Rh(100). This is consistent with the general consensus that as the metal d occupancy increases, the covalent bonding ability of the metal surface decreases. For a particular species, the geometrical parameters are similar on Pd, Rh, and Pt. As expected, the equilibrium distance perpendicular to the surface decreases in the order NH_3 > NH_2 > NH > N, being smaller for the (100) surfaces than for the (111) surfaces (Table 1). It is interesting to note that in the case of Pd(100), N is coplanar with the surface. This draws parallels to other N/metal systems, such as N on Ni(100).[53]

3.3. Adsorption of H Species. An accurate description of the adsorption properties of H is relevant to this study because the energy of the H−metal system is necessary to compute and compare the relative stabilities of the NH_x moieties (eq 2). Besides, the structure of the transition states can be strongly influenced by the different stability of atomic hydrogen on the various surface sites. Table 2 summarizes the present results. As it is well established in the literature,[54−57] the hollow fcc is always the most stable adsorption site for H on the (111) surfaces. In the case of Pt(111), all of the sites are energy minima. On the other hand, on Pd(111) the top and bridge sites are second-order and first-order stationary points, respectively, and on Rh(111) the bridge site is a saddle point. In all of the cases, the difference between hcp and fcc sites is very small (<4 kJ mol^{-1}), and diffusion from a hollow site to another one should occur across the bridge sites. The picture for the (100) plane is similar. On Pt(100), the on top and bridge sites are minima, whereas the hollow site is a second-order saddle point. The bridge site corresponds to the absolute minimum. This has also been found using a semiempirical theoretical approach,[58] although no clear experimental evidence has so far confirmed this result.[59] On Pd(100) and Rh(100), the hollow site is the most stable one in agreement with previous theoretical and experimental studies.[60−63] On both metal surfaces, the top site is a second-order stationary point.

3.4. Dehydrogenation Reactions. The adsorption energy of the NH_x species on the metals with respect to the same species

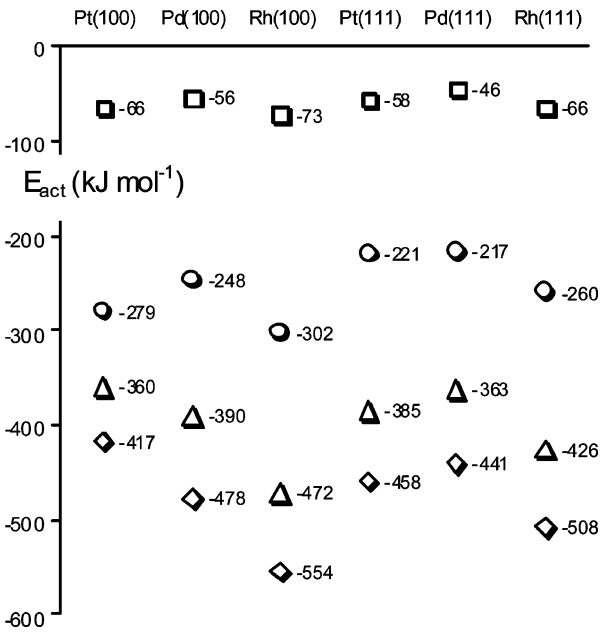

Figure 1. Adsorption energy (kJ mol^{-1}, ZPE included) of the different fragments (□, NH_3; ○, NH_2; Δ, NH; ◇, N) with respect to each species in the gas phase.

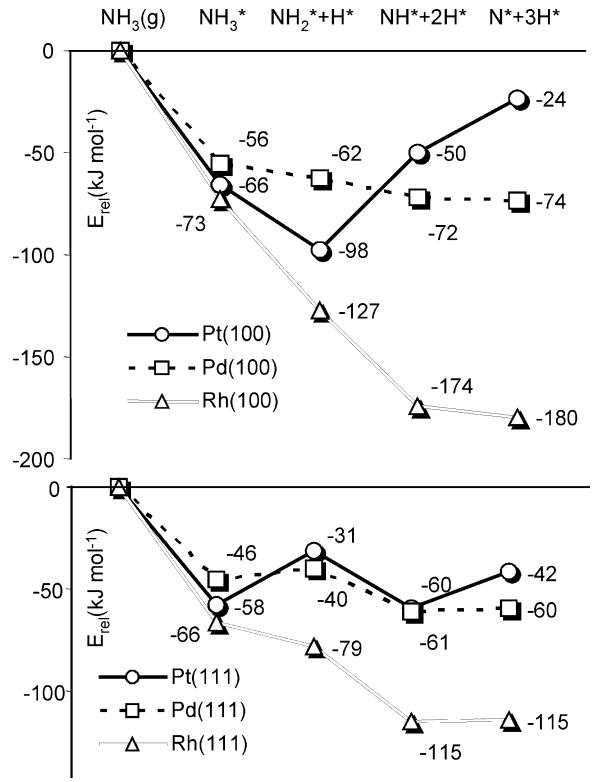

Figure 2. Relative adsorption energy (E_{rel} in kJ mol^{-1}, ZPE included) of the NH_x species with respect to gas-phase NH_3.

in the gas phase increases in the order NH_3 < NH_2 < NH < N (Table 1 and Figure 1). As expected, this trend coincides with the increasing instability of these species in the gas phase. We recomputed the adsorption energies using eq 2. The results, shown in Figure 2, clearly evidence that adsorbed NH_2 + H is more stable than adsorbed NH_3 on Pt(100), Rh(100), and Rh-(111), while the contrary applies on the other surfaces. Moreover, the NH and N moieties are strongly stabilized on Rh. In view of the relative stability of the different ammonia fragments, we can suggest that NH_2 is the predominant

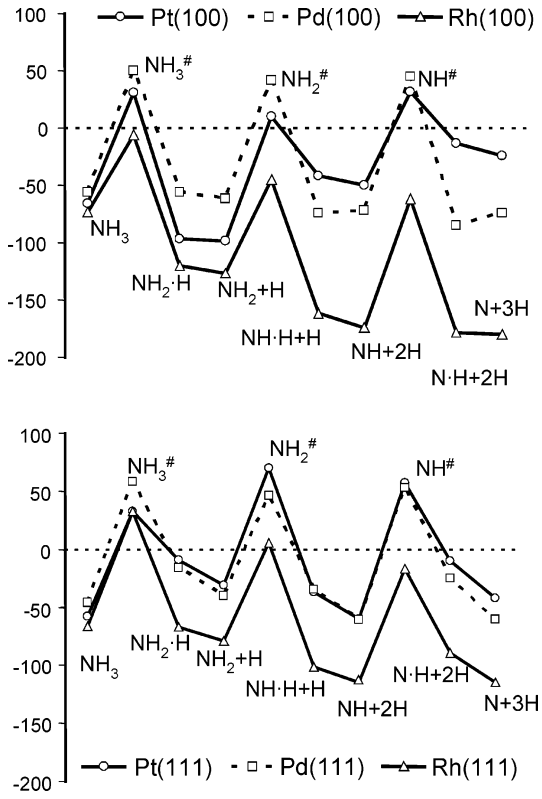

Figure 3. Reaction pathway for NH_3 dehydrogenation on the (100) and (111) surfaces. Energies in kJ mol^{-1}, ZPE included.

intermediate species during ammonia dehydrogenation on Pt(100). For Pd(100), Pt(111), and Pd(111), all of the dehydrogenated species exhibit a similar stability, and they are expected to equivalently populate the catalyst surface. In the case of Rh(100) and Rh (111), NH and N are much more stable than NH_2. Thus, rhodium surfaces strongly stabilize the presence of highly dehydrogenated products.

Figure 3 displays the schematic reaction energy profile for the successive dehydrogenation steps. For each step, the starting point was a $NH_{(3-x)}$ species ($x = 0, 1, 2$) plus x adsorbed H atoms without lateral interactions. The final state was taken as $NH_{(3-x-1)}$ plus one H atom coadsorbed on the same 2×2 unit cell in their most stable configuration and x adsorbed H atoms at infinite distance. The energy of $NH_{(3-x-1)}$ plus $(x + 1)$ coadsorbed hydrogen atoms at infinite distance as the starting point for the following step was considered. The reaction profiles are similar on the (111) surfaces, although all of the species are highly stabilized on Rh. On the other hand, when considering the (100) surfaces, Pt behaves in a singular way. The NH and N species are less stabilized than expected. The difference between Pt(100) and Pt(111) and the different stability of NH_2 compared with NH and N are in very good agreement with the recent results by Rosca and Koper.[35] These authors have related the relatively high electrocatalytic activity of Pt(100) for ammonia oxidation to dinitrogen to its ability to stabilize the NH_2 adsorbate.

Figure 4 presents the geometry of initial, transition, and final states corresponding to the most stable situation on the 2×2 unit cell for all of the elemental dehydrogenation reactions. Various transition states were identified for several reactions, as reported in the literature.[28,33] This is attributed to different possibilities for hydrogen migration. For the sake of conciseness, we only report here results for the most stable transition state in each reaction.

Table 3 summarizes the geometrical parameters, the energy barriers, and the reaction energies for all of the reactions and surfaces studied. The zero point energy (ZPE) correction changes the activation barriers significantly (15−25 kJ mol^{-1}). This is due to the loss of a N−H bond in the transition state. The huge N−H frequency evolves to an imaginary one. Accordingly, this case further exemplifies the importance of the ZPE term in computational studies. The various elementary steps will be further analyzed below.

$NH_3 \rightarrow NH_2 + H$. The lowest activation energy for the first proton abstraction of ammonia corresponds to Rh(100). The other values lie in the range 91−106 kJ mol^{-1}. On the (111) plane, the geometry of the transition state is different on the three metals studied. On Pt(111), both the NH_2 fragment and the H atom remain on a top position. On Pd(111) and Rh(111), the H atom is close to a bridge position. On the other hand, the final state corresponds to a NH_2 species adsorbed on a bridge position and the H atom on the neighboring fcc site. Our results on the Pt(111) surface are in line with those recently reported by Offermans et al.[31] and Michaelides and Hu.[64] In the case of Rh(111), the geometry of the transition state is close to the one reported by Liu et al.[33] These authors have studied the reverse hydrogenation reactions on Rh(111). They have reported a barrier of 120 kJ mol^{-1} for the $NH_2 + H \rightarrow NH_3$ reaction, which is coincident with the value determined from our present calculations. On the (100) surfaces, the geometry of the transition state is roughly the same for Pt, Pd, and Rh (see Figure 4). The NH_2 moiety is always positioned on a bridge site, while the H atom sits on top. In the final state, the NH_2 remains on the bridge site and the hydrogen atom gets adsorbed on a bridge site of Pt and Pd and on a 4-fold hollow site on Rh.

$NH_2 \rightarrow NH + H$. Similarly to the first dehydrogenation, the reaction barriers of the second dehydrogenation step lie in a narrow range (see Table 3). Again, the Rh(100) surface leads to the lowest activation energy. On the (100) surfaces, the geometries of the transition states are very similar, the NH fragment stays in the vicinity of a bridge site, whereas H is close to the nearest parallel bridge site. The barriers are similar for Pt and Pd and lower for Rh. The reaction is endothermic for Pt, athermic for Pd, and exothermic for Rh. On the (111) surfaces, the geometry of the lowest energy transition state is different on the three metals. On Pt, the NH species remains on the bridge position and H moves to the nearest top position. On Pd and Rh, the NH fragment moves to a fcc (Pd) or to a hcp position (Rh), whereas the H atom shifts to fcc (Pd) or top (Rh). These results find correspondence with Offermans et al.[31] on Pt(111), Crawford and Hu[28] on Pd(111) and Rh(111), and Liu and co-workers[33] on Rh(111). Our geometric parameters are in line with those previously reported. The only difference arises from the position of the H atom on Pd. Crawford and Hu[28] have found that H adsorbs close to a hcp position, whereas our calculations predicted a fcc adsorption site. The activation energies are also in good agreement with the results of Offermans et al.[31] and Liu and co-workers.[33] Unfortunately, the reaction barriers were not reported in ref 28.

$NH \rightarrow N + H$. The activation energy of the last dehydrogenation step is the highest one for all of the metal surfaces except for Pt(100). The reaction barrier over Pt(100) is relatively low (82 kJ mol^{-1}) as compared to the activation energies on Pd and Rh (118 and 113 kJ mol^{-1}, respectively). On Pt(100), the transition state is similar to the one for NH_2, NH and H being close to two parallel bridge positions. However, on Pd(100) and Rh(100), the N atom reaches the hollow position with the H atom close to a top site. Interestingly, for Pd(100), a "clock"

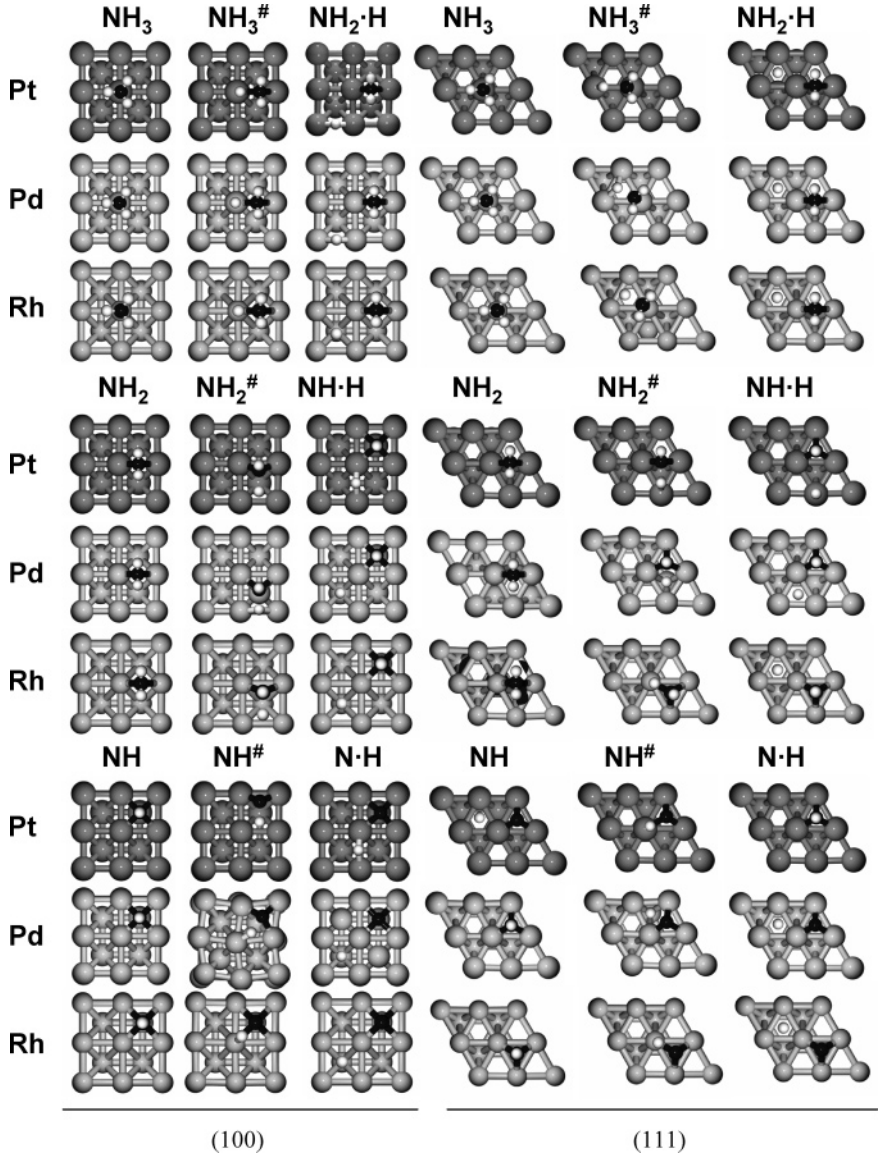

Figure 4. Top view of the initial, transition, and final states for the dehydrogenation reactions on the (100) and (111) metal surfaces.

reconstruction of the surface was obtained similar to that reported for N on Ni(100).[65]

For Pt(111) and Rh(111), the N fragment and the H atom in the most stable transition state lie on hollow and top positions, respectively, as reported by Offermans et al.[31] and Liu et al.[33] For Pd(111), the transition state with H in a position intermediate between hcp and bridge is the preferred one. This is also in agreement with the results from Crawford and Hu.[28]

3.5. Microkinetics. Table 4 gives the pre-exponential factors and rate coefficients at selected temperatures, as determined by eq 4. These results have to be considered semiquantitative due to the several approximations used in the theoretical treatment (the density functional, the reduced number of layers in the slab model, the harmonic approximation, and the fact that the surface phonons were neglected in the frequency calculations).

On the (100) surfaces, NH_3 dissociates much easier on Rh than on Pt or Pd, the latter two being very similar. For the NH_2 dissociation, a similar trend was obtained. However, this tendency is not followed by NH. The last dehydrogenation is more favorable over Pt, followed by Rh and Pd. On the basis of these results, we can suggest that the first dehydrogenation is the rate-determining step on Pt(100) and Pd(100). On the other hand, on Rh(100), the first step is relatively fast and the $NH \rightarrow N + H$ step limits the reaction rate. On the (111) surfaces, the trends are similar. Nevertheless, the differences between the reaction rates lie in a narrow range.

Interestingly, the trends that could be extracted from the simple analysis of the activation energies are modulated when including the effect of temperature, especially for the first dehydrogenation step. This illustrates the importance of taking into account the statistical thermodynamics in reactivity studies. This is because adsorbed NH_3 presents higher configurational entropy than the activated complex due to the nearly free rotation of NH_3 adsorbed on top site. As a consequence, the pre-exponential factors for the first dehydrogenation step are the lowest ones.

The decomposition of NH_3 into N_2 and H_2 has been investigated over polycrystalline Pt, Rh, and Pd wires in a differential flow reactor, at pressures from 0.01 to 1 Torr and temperatures from 500 to 1900 K.[48] It has been found that Rh is more active than Pt and Pd and that the rate of product formation can be described by a Langmuir−Hinshelwood unimolecular model. The determined heats of NH_3 adsorption are very similar over the three metals (67−71 kJ mol^{-1}). However, Pd (109 kJ mol^{-1}) exhibited a higher apparent activation energy than did Pt and Rh (88 kJ mol^{-1}). Thus, the

TABLE 3: Geometries of the Transition States, Activation Energy Barriers (E_{act}), and Reaction Energies with Respect to the coadsorbed Fragments on the 2 × 2 Cell in the Most Stable Configuration (ΔE_1), and with Respect to the Sum of the Binding Energies of the Isolated Fragments in Their Most Stable Adsorption Site (ΔE_2)[a]

	Pt(100)	Pd(100)	Rh(100)	Pt(111)	Pd(111)	Rh(111)
			$NH_3 \rightarrow NH_2 + H$			
E_{act}	97	106	67	91	104	100
ΔE_1	−31	0	−47	49	30	0
ΔE_2	−32	−7	−54	26	6	−12
site N	bridge	bridge	bridge	top[b]	top[b]	top[b]
site H	top[b]	top	top	top[b]	bridge[b]	bridge[b]
d_{M-N}	2.33	2.18	2.18	2.04	2.04	2.03
d_{N-H}	1.49	1.59	1.43	1.90	1.77	1.69
d_{M-H}	1.62	1.59	1.65	1.60	1.79	1.87
			$NH_2 \rightarrow NH + H$			
E_{act}	107	104	82	101	86	84
ΔE_1	56	−12	−35	−5	5	−22
ΔE_2	48	−10	−47	−28	−21	−36
site N	bridge[b]	hollow[b]	bridge[b]	bridge	fcc[b]	hcp
site H	bridge[b]	bridge	bridge[b]	top[b]	hcp	top[b]
d_{M-N}	2.00	2.08	1.96	2.03	2.04	2.09
d_{N-H}	1.64	1.52	1.57	1.68	1.43	1.41
d_{M-H}	1.88	1.75	1.84	1.62	2	1.66
			$NH \rightarrow N + H$			
E_{act}	82	118	113	116	114	98
ΔE_1	37	−13	−4	50	36	26
ΔE_2	26	−1	−5	18	1	1
site N	bridge[b]	hollow[b]	hollow[b]	fcc	fcc	hcp
site H	bridge[b]	hollow[b]	top[b]	top[b]	hcp	top[b]
d_{M-N}	1.92	1.94	2.13	2.11	1.98	2.03
d_{N-H}	1.53	1.48	1.53	1.52	1.42	1.51
d_{M-H}	1.90	1.70	1.65	1.63	1.89	1.63

[a] Energies in kJ mol^{-1} include the ZPE. Distances in angstroms. [b] Sites slightly displaced with respect to the symmetric site.

TABLE 4: Pre-exponential Factors (k^0, s^{-1}), Activation Energies (E_{act}, kJ mol^{-1}), and Rate Coefficients (k_v, s^{-1}) at 300, 500, and 700 K for the Three Successive Elementary Steps Involved in Ammonia Dehydrogenation

	k^0				k_v		
	300	500	700	E_{act}	300	500	700
			Pt(100)				
$NH_3 \rightarrow NH_2 + H$	2.5×10^{11}	3.7×10^{11}	5.1×10^{11}	97	5.5×10^{-6}	36	3.6×10^{4}
$NH_2 \rightarrow NH + H$	5.0×10^{12}	9.3×10^{12}	1.4×10^{13}	107	9.8×10^{-7}	55	1.4×10^{5}
$NH \rightarrow N + H$	4.9×10^{12}	7.4×10^{12}	9.9×10^{12}	82	3.0×10^{-2}	2.2×10^{4}	8.0×10^{6}
			Pd(100)				
$NH_3 \rightarrow NH_2 + H$	1.8×10^{11}	2.4×10^{11}	3.1×10^{11}	106	7.8×10^{-8}	2.3	4.1×10^{3}
$NH_2 \rightarrow NH + H$	4.9×10^{12}	7.3×10^{12}	9.5×10^{12}	104	3.8×10^{-6}	99	1.6×10^{5}
$NH \rightarrow N + H$	6.0×10^{12}	9.7×10^{12}	1.3×10^{13}	118	1.9×10^{-8}	4.9	2.2×10^{4}
			Rh(100)				
$NH_3 \rightarrow NH_2 + H$	2.5×10^{11}	3.1×10^{11}	3.9×10^{11}	67	5.7×10^{-1}	3.3×10^{4}	4.1×10^{6}
$NH_2 \rightarrow NH + H$	4.3×10^{12}	6.7×10^{12}	9.3×10^{12}	82	2.6×10^{-2}	2.0×10^{4}	7.5×10^{6}
$NH \rightarrow N + H$	8.3×10^{12}	1.6×10^{13}	2.3×10^{13}	113	2.0×10^{-7}	27	9.1×10^{4}
			Pt(111)				
$NH_3 \rightarrow NH_2 + H$	4.6×10^{11}	7.1×10^{11}	1.0×10^{12}	91	6.1×10^{-5}	2.1×10^{2}	1.5×10^{5}
$NH_2 \rightarrow NH + H$	5.8×10^{12}	1.1×10^{13}	1.6×10^{13}	101	1.3×10^{-5}	2.2×10^{2}	3.1×10^{5}
$NH \rightarrow N + H$	7.2×10^{12}	1.3×10^{13}	1.9×10^{13}	116	4.1×10^{-8}	9.3	3.9×10^{4}
			Pd(111)				
$NH_3 \rightarrow NH_2 + H$	4.9×10^{11}	8.5×10^{11}	1.3×10^{12}	104	4.2×10^{-7}	12	2.4×10^{4}
$NH_2 \rightarrow NH + H$	4.0×10^{12}	5.8×10^{12}	7.8×10^{12}	86	3.9×10^{-3}	5.7×10^{3}	2.9×10^{6}
$NH \rightarrow N + H$	7.9×10^{12}	1.6×10^{13}	2.7×10^{13}	114	9.6×10^{-8}	18	7.9×10^{4}
			Rh(111)				
$NH_3 \rightarrow NH_2 + H$	7.3×10^{11}	1.5×10^{12}	2.7×10^{12}	100	3.3×10^{-6}	59	9.8×10^{4}
$NH_2 \rightarrow NH + H$	5.6×10^{12}	9.0×10^{12}	1.2×10^{13}	84	1.2×10^{-2}	1.4×10^{4}	6.2×10^{6}
$NH \rightarrow N + H$	7.1×10^{12}	1.2×10^{13}	1.6×10^{13}	98	5.8×10^{-5}	6.8×10^{2}	7.8×10^{5}

experimentally determined order of activity between the metals is excellently supported by our calculations. The higher activity of Rh over Pt and Pd is due to the lower activation barrier for the $NH_3 \rightarrow NH_2$ reaction as well as to the enhanced stabilization of the various intermediates involved.

3.6. Energy Relationships. It has long been realized that the potential energy of the transition state with respect to the adsorbed molecule in the gas phase (E_{TS}) and the adsorption energy (E_{ads}) of the final products with respect to the same reference are often correlated.[64−67] This Brønsted−Evans−Polany (BEP)-type relationship also applies in the present study where $E_{TS} = 0.99E_{ads} + 107$ (in kJ mol^{-1}) with $R^2 = 0.977$ (see Figure 5). Interestingly, this correlation is very similar to the one found by Nørskov et al.[66] for N_2, CO, NO, and O_2

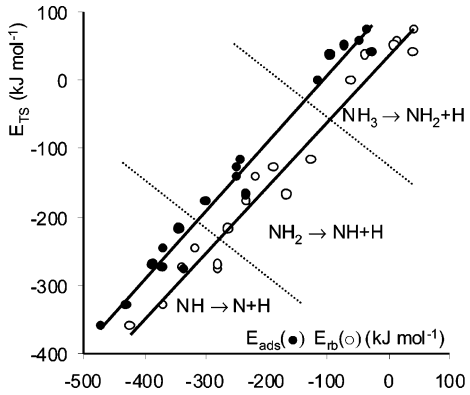

Figure 5. Transition state potential energy (E_{TS}) versus the adsorption energy of the reaction products (E_{ads}, ●) and rebonding energy (E_{rb}, ○) for all of the transition states computed in this work. For each point, the zero-energy reference is the one of each reacting species in the gas phase.

dissociation on several metal surfaces. These authors have proposed that this can be linked to the fact that the bond length in the transition state is quite long. Therefore, the variation in the energy of the transition state follows that of the final state, and it gives a linear relationship between these two energies with a slope close to the unity. Loffreda et al.[67] have found similar trends for NO dissociation. They have shown that the transition state is "late" on the reaction path and concluded that the stability of the transition state and the value of the barrier are governed by the strength of the atom surface interaction, that is, by the stability of the final coadsorbed N + O state. All of the dehydrogenation steps of the present study follow similar trends. In all of the cases, the elongated N−H bond in the transition state is nearly broken (see Table 3). However, the above correlation should be taken with caution because it depends strongly on the adsorption energy of each reacting species. In fact, the correlation (R^2) for each single step is much lower than 0.9 ($R^2 = 0.584$, 0.670, and 0.783 for the consecutive dehydrogenation reactions). Interestingly, we did not obtain a significant correlation between the activation energy barriers and the reaction energies. This result has yet been reported by Offermans et al.[31] These authors have found a trend in the activation energy versus the reaction energy of dehydrogenation reactions on Pt(111), but a linear relationship is not applicable in an useful way. Hammer[68] has proposed another relationship between the calculated adsorption energy of the transition state and the "rebonding energy", E_{rb}, defined as the sum of the individual chemisorption energies of the final fragments in the geometry of the transition state. With this definition, $E_{TS} = E_{rb} + E_{int}$, where E_{int} is the intramolecular repulsive interaction of the fragments in the transition state. The correlation between E_{rb} and E_{TS} is also presented in Figure 5: $E_{TS} = 0.96E_{rb} + 35.8$ ($R^2 = 0.968$). This correlation shows that, although E_{int} is not constant, the variations remain small. All of these relationships represent only qualitative trends because a particular elementary step may deviate considerably from the relation. They may be useful to estimate apparent activation energies from adsorption energies. However, our results further confirm that the Brønsted−Evans−Polany relationship should be analyzed for any particular problem.

4. Conclusions

Using periodic slab DFT calculations, we have successfully computed the geometry, site preference, and relative stability of adsorbed ammonia and its dehydrogenated fragments (NH_2, NH, N) on the (100) and (111) surfaces of Pd, Rh, and Pt. The adsorption energy is higher on the more open (100) plane than on the (111) one for all of the metals. Moreover, the adsorption energies are stronger on Rh than on Pd or Pt. On the six metal surfaces, NH_3 adsorbs on top sites, NH_2 on bridge, and NH and N on hollow sites. The N−H and M−N distances are similar for all of the species. The differences between the three metals are more significant on the (100) than on the (111) surfaces. The transition states and reaction barriers for the successive dehydrogenation steps have also been determined. All of the barriers range between 67 kJ mol^{-1} ($NH_3 \rightarrow NH_2 + H$ on Rh(100)) and 118 kJ mol^{-1} ($NH \rightarrow N + H$ on Pd(100)). As a general trend, the barriers are higher for the last dehydrogenation step (except for Pt(100)). However, once the kinetic constants are computed, the rate-determining step corresponds to the first hydrogen abstraction (except for Rh(100)) due to the negative activation entropy of this step. On Pd(111) and Pt(111), all of the transition states are above the energy of NH_3 in the gas phase, while on Rh(111) all of the species are more stable than adsorbed ammonia. On the (100) surfaces, the energy of the different adsorbed intermediates and transition states is higher on Pt and Pd than on Rh. It is also seen that in the case of Rh, all of the transition states are below the energy of gas-phase NH_3. Thus, according to our calculations, Rh should be a more active catalyst for NH_3 decomposition than Pt or Pd, in agreement with experimental results reported in the literature. We have found a linear relationship between the transition state potential energy and the adsorption energy of the final state for the set of dehydrogenation reactions. However, a significant correlation between the activation energies and the reaction energies has not been obtained. Therefore, the original Brønsted−Evans−Polany relationship cannot be taken as a universal rule in heterogeneous catalysis.

Acknowledgment. We thank financial support from the Spanish Ministry for Science and Education (projects CTQU2005-08459-C02-02 and CTQ2006-01562/PPQ) and the Catalan government (2005SGR-00104). G.N.-L. is indebted to Universitat Rovira i Virgili for a predoctoral grant. Part of the computer time was provided by the CESCA/CEPBA supercomputer centers. We are indebted to Drs. D. Curulla and D. Loffreda for fruitful discussions.

References and Notes

(1) *Catalytic Ammonia Synthesis: Fundamentals and Practice*; Jennings, J. R., Ed.; Plenum Press: New York, 1991.
(2) *Ullmann's Encyclopedia of Industrial Chemistry*, 7th ed.; Wiley−VCH Verlag GMBH: Weinheim, 2005.
(3) Satterfield, C. N. *Heterogeneous Catalysis in Industrial Practice*, 2nd ed.; McGraw-Hill: New York, 1991.
(4) Choudhary, T. V.; Sivadinarayana, C.; Goodmann, D. W. *Catal. Lett.* **2001**, *72*, 1.
(5) Yin, S. F.; Xu, B. Q.; Zhou, X. P.; Au, C. T. *Appl. Catal., A* **2004**, *277*, 1.
(6) Christensen, C. H.; Johannessen, T.; Sørensen, R. Z.; Nørskov, J. K. *Catal. Today* **2006**, *111*, 140.
(7) Gland, J. L.; Korchak, V. N. *J. Catal.* **1978**, *53*, 9.
(8) Gland, J. L.; Woodward, G. C. *J. Catal.* **1980**, *61*, 543.
(9) Sexton, B. A.; Mitchell, G. E. *Surf. Sci.* **1980**, *99*, 523.
(10) Asscher, M.; Guthrie, W. L.; Lin, T.-H.; Somorjai, G. A. *J. Phys. Chem.* **1984**, *88*, 3233.
(11) Mieher, W. D.; Ho, W. *Surf. Sci.* **1995**, *322*, 151.
(12) Bradley, J. M.; Hopkinson, A.; King, D. A. *J. Phys. Chem.* **1995**, *99*, 17032.
(13) Bradley, J. M.; Hopkinson, A.; King, D. A. *Surf. Sci.* **1997**, *371*, 255.
(14) Kim M.; Pratt, S. J.; King, D. A. *J. Am. Chem. Soc*. **2000**, *122*, 2409.
(15) Pérez-Ramírez, J.; Kondratenko, E. V. *Chem. Commun*. **2004**, *376*.

(16) Pérez-Ramírez, J.; Kondratenko, E. V.; Kondratenko, V.; Baerns, M. *J. Catal.* **2004**, *227*, 90.
(17) Pérez-Ramírez, J.; Kondratenko, E. V.; Kondratenko, V.; Baerns, M. *J. Catal.* **2005**, *229*, 303.
(18) Zemlyanov, D. Y.; Smirnov, M. Y.; Gorodetskii, V. V. *Surf. Sci.* **1997**, *391*, 37.
(19) Sun, Y.-M.; Sloan, D.; Ihm, H.; White, J. M. *J. Vac. Sci. Technol., A* **1996**, *14*, 1516.
(20) Bater, C.; Campbell, J. J.; Craig, J. J., Jr. *Surf. Interface Anal.* **1998**, *26*, 97.
(21) Yamada, T.; Tanaka, K. *J. Am. Chem. Soc.* **1989**, *111*, 6880.
(22) Tanaka, K.; Yamada, T.; Nieuwenhuys, B. E. *Surf. Sci.* **1991**, *242*, 503.
(23) Yamada, T.; Hirano, H.; Tanaka, K.; Siera, J.; Nieuwenhuys, B. E. *Surf. Sci.* **1990**, *226*, 1.
(24) Yamada, T.; Tanaka, K. *J. Am. Chem. Soc.* **1991**, *113*, 1173.
(25) Herzeg, E.; Mudiyanseage, K.; Trenary, M. *J. Phys. Chem. B* **2005**, *109*, 2828.
(26) Logadóttir, A.; Nørskov, J. K. *J. Catal.* **2003**, *220*, 273.
(27) Zhang, C. J.; Lynch, M.; Hu, P. *Surf. Sci.* **2002**, *496*, 221.
(28) Crawford, P.; Hu, P. *J. Chem. Phys.* **2006**, *124*, 044705.
(29) Baerns, M.; Imbihl, R.; Kondratenko, V. A.; Kraehnert, R.; Offermans, W. K.; van Santen, R. A.; Scheibe, A. *J. Catal.* **2005**, *232*, 226.
(30) Novell-Leruth, G.; Valcárcel, A.; Clotet, A.; Ricart, J. M; Pérez-Ramírez, J. *J. Phys. Chem. B* **2005**, *109*, 18061.
(31) Offermans, W. K.; Jansen, A. P. J.; van Santen, R. A. *Surf. Sci.* **2006**, *24*, 1714.
(32) Stolbov, S.; Rahman, T. S. *J. Chem. Phys.* **2005**, *123*, 204716.
(33) Liu, Z.-P.; Hu, P.; Lee, M.-H. *J. Chem. Phys.* **2003**, *119*, 6282.
(34) Vidal-Iglesias, J. F.; García-Aráez, N.; Montiel, V.; Feliu, J. M.; Aldaz, A. *Electrochem. Commun.* **2003**, *5*, 22.
(35) Rosca, V.; Koper, M. T. M. *Phys. Chem. Chem. Phys.* **2006**, *8*, 2513.
(36) Kresse, G.; Hafner, J. *Phys. Rev. B* **1993**, *47*, 558.
(37) Kresse, G.; Furthmüller, J. *Phys. Rev. B* **1996**, *54*, 11169.
(38) Kresse, G.; Joubert, D. *Phys. Rev. B* **1998**, *59*, 1758.
(39) Perdew, J. P.; Wang, Y. *Phys. Rev. B* **1992**, *45*, 13244.
(40) Wyckoff, R. W. G. *Crystal Structures*, 2nd ed.; Interscience: New York, 1965; Vol. 1.
(41) Henkelman, G.; Jónsson, H. *J. Chem. Phys.* **1999**, *111*, 7010.
(42) Fahmi, A.; van Santen, R. A. *Z. Phys. Chem.* **1996**, *197*, 203.
(43) García-Hernández, M.; López, N.; Moreira, I. P. R.; Paniagua, J. C.; Illas, F. *Surf. Sci.* **1999**, *43*, 18.
(44) Fierro, C. *J. Phys. Chem.* **1998**, *92*, 4401.
(45) Chattopadhyay, A.; Yang, H.; Witten, J. L. *J. Phys. Chem.* **1990**, *9*, 6379.
(46) Neurock, M.; van Santen, R. A.; Biemolt, W.; Jansen, A. P. J. *J. Am. Chem. Soc.* **1994**, *116*, 6860.
(47) Frechard, F.; van Santen, R. A.; Siokou, A.; Niemantsverdriet, J. W.; Hafner, J. *J. Chem. Phys.* **1999**, *111*, 8124.
(48) Papapolymerou, G.; Bontozoglou, V. *J. Mol. Catal. A: Chem.* **1997**, *120*, 165.
(49) Ample, F.; Clotet, A.; Ricart, J. M.; Curulla, D.; Niemantsverdriet, J. W. *Chem. Phys. Lett.* **2004**, *385*, 52.
(50) Mavrikakis, M.; Rempel, J.; Greeley, H.; Hansen, L. B.; Nørskov, J. K. *J. Chem. Phys.* **2002**, *117*, 6737.
(51) Mei, D.; Ge, Q.; Neurock, M.; Kieken, L.; Lerou, J. *Mol. Phys.* **2004**, *20*, 361.
(52) Ford, D. C.; Xu, Y.; Mavrikakis, M. *Surf. Sci.* **2005**, *587*, 159.
(53) Daum, W.; Lehwald, S.; Ibach, H.; Rahman, T. S. *Phys. Rev. B* **1987**, *35*, 9510.
(54) Olsen, R. A.; Kroes, G. J.; Baerends, E. J. *J. Chem. Phys.* **1999**, *111*, 11155.
(55) Pallassana, V.; Neurock, M.; Hansen, L. B.; Hammer, B.; Nørskov, J. K. *Phys. Rev. B* **1999**, *60*, 6146.
(56) Mitsui, T.; Rose, M. K.; Fomin, E.; Ogletree, D. F.; Salmerón, M. *Surf. Sci.* **2003**, *540*, 5.
(57) Dong, W.; Ledentu, V.; Sautet, P.; Eichler, A.; Hafner, J. *Surf. Sci.* **1998**, *411*, 123.
(58) Zinola, C. F.; Arvia, A. J. *Electrochim. Acta* **1996**, *41*, 2267.
(59) Hu, X.; Lin, Z. *Phys. Rev. B* **1995**, *52*, 11467.
(60) Lovvik, O. M.; Olsen, R. A. *J. Chem. Phys.* **2003**, *118*, 3268.
(61) Eichler, A.; Hafner, J.; Kresse, G. *J. Phys.: Condens. Matter* **1996**, *8*, 7659.
(62) Pauer, G.; Eichler, A.; Sock, M.; Ramsey, M. G.; Netzer, F.; Wingler, A. *J. Chem. Phys.* **2003**, *119*, 5253.
(63) Klein, C.; Eichler, A.; Hebenstreit, E. L. D.; Pauer, G.; Koller, R.; Winkler, A.; Schmid, M.; Varga, P. *Phys. Rev. Lett.* **2003**, *90*, 176101-1.
(64) Michaelides, A.; Hu, P. *J. Am. Chem. Soc.* **2000**, *122*, 9866.
(65) Kirsch, J. E.; Harris, S. *Surf. Sci.* **2003**, *522*, 125.
(66) Nørskov, J. K.; Bligaard, T.; Logadottir, A.; Bahn, S.; Hansen, L. B.; Bollinger, M.; Bengaard, H.; Hammer, B.; Sljivancanin, Z.; Mavrikakis, M.; Xu,, Y.; Dahl, S.; Jacobsen, C. J. H. *J. Catal.* **2002**, *209*, 275.
(67) Loffreda, D.; Delbecq, F.; Simon, D.; Sautet, F. *J. Chem. Phys.* **2001**, *17*, 8101.
(68) Hammer, B. *Surf. Sci.* **2000**, *459*, 323.